Journal of Renewable Energy and Environment

Research Article

Journal Homepage: www.jree.ir

The Effect of Proton-Exchange Membrane Fuel Cell Configuration Changing from Straight to Cylindrical State on Performance and Mass Transport: Numerical Procedure

Tuhid Pashaee Golmarz[a], Sajad Rezazadeh[a*], Maryam Yaldagard[b], Narmin Bagherzadeh[a]

[a] *Department of Renewable Energies, School of Mechanical Engineering, Urmia University of Technology, P. O. Box: 57166-17165, Urmia, West Azerbaijan, Iran.*
[b] *Department of Engineering, School of Chemical Engineering, Urmia University, P. O. Box: 57561-51818, Urmia, West Azerbaijan, Iran.*

PAPER INFO

Paper history:
Received 02 November 2020
Accepted in revised form 15 February 2021

Keywords:
PEM Fuel Cell,
Geometry,
Mass Transport,
Performance

ABSTRACT

In the present work, a Proton-Exchange Membrane Fuel Cell (PEMFC) as a three-dimensional and single phase was studied. Computational fluid dynamics and finite volume technique were employed to discretize and solve a single set of flow fields and electricity governing equations. The obtained numerical results were validated with valid data in the literature and good agreement was observed between them. The main purpose of this paper is to investigate the effect of deformation of the geometric structure of a conventional cubic fuel cell into a cylindrical one. For this purpose, some important parameters indicating the operation of the fuel cell such as oxygen distribution, water, hydrogen, proton conductivity of the membrane, electric current density, and temperature distribution for two voltage differences between the anode and cathode and the proposed models were studied in detail. Numerical results showed that in the difference of voltages studied, the proposed new model had better performance than the conventional model and had a higher current density, in which at V = 0.4 [V], about a 10.35 % increase in the amount of electric current density was observed and the average increment in generated power was about 8 %, which could be a considerable value in a stack of cells. Finally, the discussion of critical parameters for both models was presented in more detail. The core idea of the results is that the Oxygen and Hydrogen utilization, water creation, and heat generation are greater in the new model.

https://doi.org/10.30501/jree.2020.253825.1152

1. INTRODUCTION

Fuel cells are some kinds of gadgets that transform the synthetic energy of vaporous or fluid reactants into electrical energy. The reactants are precluded from chemically reacting by isolating them with an electrolyte. This layer is in connection with permeable electrode parts. Additionally, the electrolyte layer interferes with the electrochemical reactions occuring at the anodes by directing a particular particle during the activity of the power device. As a standard power module, a proton or oxide particle current is passed through the electrolyte and parts of the heterogeneous anode and cathode structures. This sort works with hydrogen and oxygen as responding gases [1]. Various specialists have zeroed in on various parts of the power device. Bernardi and Verbrugge [2, 3] examined a one-dimensional model giving worthy outcomes about the electrochemical responses and transport marvels in energy units. Fuller and Newman [4] investigated a straightforward model of the film anode. They studied the fixation arrangement hypothesis for the film and warm impacts. Nguyen and White [5] spoke to a two-dimensional model. They chipped away at electro-assimilation drag power just as warmth moved from the strong stage to the gas stage through the stream channels for water transport marvels. Dutta et al. examined a three-dimensional type of PEMFC [6]. Berning et al. built up a consistent state, three-dimensional, non-isothermal model to foresee PEM energy component responses [7]. Yang et al. [8] expanded the exhibition of a PEM energy unit. Such high force densities are achieved through better usage of Pt crystallites in the response layer. This improved presentation can be accomplished by making a flimsy impetus layer on the film surface. The power in the front surface impetuses is too basic to limit the coagulation of Pt particles when the energy units are exposed to long haul activity. Some other authors tested variable numerical methods to check the capability of these types of procedures like Akbari et al. [9] and Carral et al. [10]. They utilized the Lattice–Boltzmann strategy to show the water bead dynamic conduct and a limited component procedure to reproduce the PEMFC stack routinely. Ahmadi et al. [11] mathematically and tentatively examined a PEM energy component. Their outcomes demonstrated that the capability of cells improved by expanding the working weight. They likewise explored the GDL mathematical setup impact on PEM energy component execution. The outcomes demonstrated an observable increment in current thickness at comparative cell voltages in

*Corresponding Author's Email: sor.mems@gmail.com (S. Rezazadeh)
URL: http://www.jree.ir/article_126342.html

Please cite this article as: Pashaee Golmarz, T., Rezazadeh, S., Yaldagard, M. and Bagherzadeh, N., "The effect of proton-exchange membrane fuel cell configuration changing from straight to cylindrical state on performance and mass transport: Numerical procedure", ***Journal of Renewable Energy and Environment (JREE)***, Vol. 8, No. 2, (2021), 39-53. (https://doi.org/10.30501/jree.2020.253825.1152).

comparison with the base model. Rezazadeh et al. [12] proposed a three-dimensional and single-stage CFD model of a PEMFC with two gas circulation stream channels and Layer Cathode Gathering (MEA). They examined the working weight impact in their paper. Also, the impact of mathematical arrangement of Gas Dissemination Layers (GDLs) on cell execution indicated that the watched model, with unmistakable GDLs, developed the cell execution and the customary model. While examination and advancement in the field of energy units have been followed, these frameworks and their applications are still amazingly perplexing and costly and are not appropriate for business use. Significant points of ongoing advancements are focused on the cost decrease and enormous volume assembling of the impetus layers, films, and bipolar plates. An explanatory arrangement is dependent on the bother strategy to fathom the progression and force conditions overseeing the stream in gas channels of a PEMFC having roundabout and curved cross-areas, as explored by Ahmadi et al. [20]. Moreover, Pashaee et al. [21] conducted a numerical investigation of bent shape channel impact on execution and circulation of species in a Proton-Trade Layer Power module.

According to the performed researches, the main focus is on the conventional form of the fuel cell (straight model) and it has been recognized that the configuration changing of the whole PEM to cylindrical state is a suitable idea for the study. Therefore, in the present work, a 3D numerical study of novel-cylindrical-cell shape effect on execution and species dispersion in a PEM fuel cell was investigated in more detail. Some important parameters such as species mass fractions, cell temperature, cathode overpotential, and electrical current density were illustrated and contrasted with the simple model outcomes. In doing so, a user can choose the best model for any certain applications. A list of nomenclature for better understanding the terms of the governing equations can be found in [18].

2. MATHEMATICAL MODEL

Figures 1 and 2 show a schematic of a solitary cell of a PEMFC (base model). It includes two permeable terminals, a polymer electrolyte film, a two-impetus layer, and two-gas distributor plates. The MEM layer is inserted between the gas channels. The present non-isothermal model includes some assumptions. The following simplifications have been applied to the governing equation defining:

- All gases are thought to be an ideal gas combination.
- The GDLs and impetus layers are homogeneously permeable.
- The stream is incompressible and laminar due to low-pressure slopes and speeds.
- The volume of fluid stage water in the space is irrelevant; thus, the stream field is a solitary phase.

3. GOVERNING EQUATIONS

In this numerical reenactment, a solitary area model formulation was applied to administering conditions. These overseeing conditions comprise mass preservation, momentum, species, and charge equations, which can be written as follows:

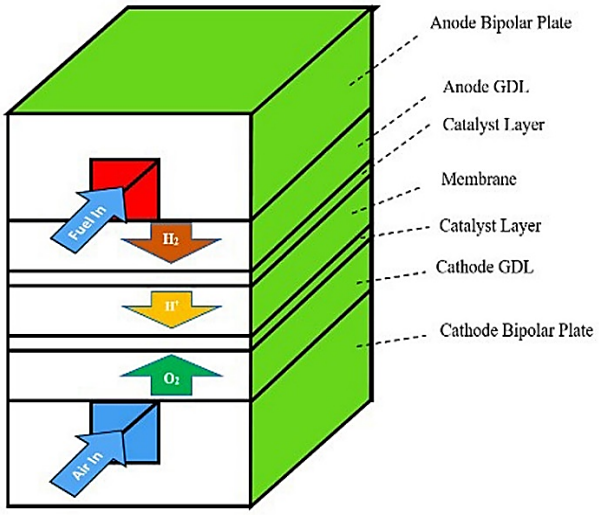

Figure 1. Simplified shape of a PEM fuel cell (base model)

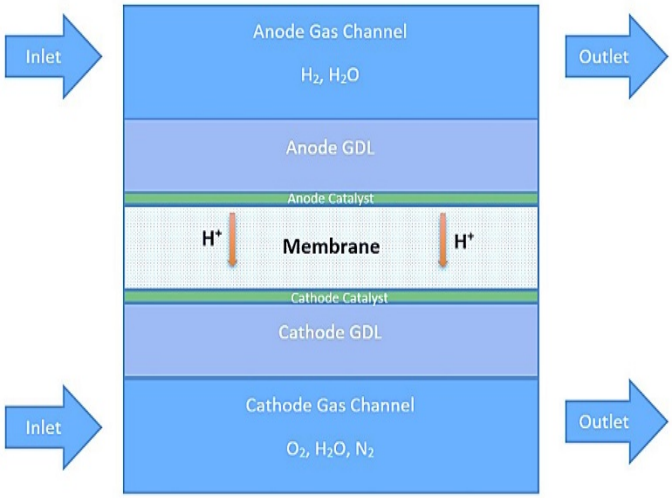

Figure 2. PEMFC in lateral view

$$(\nabla.\rho u) = 0 \tag{1}$$

$$\frac{1}{(\varepsilon^{eff})^2}\nabla.(\rho uu) = -\nabla P + \nabla.(\mu\nabla u) + S_u \tag{2}$$

$$\frac{1}{(\varepsilon^{eff})^2}\nabla.(\rho uu) = -\nabla P + \nabla.(\mu\nabla u) + S_u \tag{3}$$

$$\nabla.(uC_k) = \nabla.\left(D_k^{eff}\nabla C_k\right) + S_k \tag{4}$$

$$\nabla.\left(K_e^{eff}\nabla\Phi_e\right) + S_\Phi = 0 \tag{5}$$

In Equation (1), the mixture density is denoted by ρ. ε is the efficient porosity entrant porous inductor, and the viscosity of the gas mixture in the momentum equation is denoted by μ as in Eq. (2). Su is the source of momentum equation term and is used to describe Darcy's drag for flow through porous gas diffusion layers and catalyst layers. More information about the governing equations and source terms is available in references [13-25].

4. BOUNDARY CONDITION

The mentioned governing equations are solved by using the boundary condition, which is shown in Table 1. Figure 3 shows the solution procedure. Accordingly, an initial voltage is introduced first. Then, all equations are solved. Finally, if the convergence criterion is met, the process ends and the current density is calculated.

Table 1. The boundary condition of the fuel cell

Boundary condition	The location
$u = u_{in}, T = T_{in}, v = 0, C_{H2} = C^{a}_{H2,in}\ ,\ C_{H2O} = C^{a}_{H2O}$	Anode channel inlet
$u = u_{in}, T = T_{in}, v = 0, C_{O2} = C^{c}_{O2,in}\ ,\ C_{N2} = C^{c}_{N2}$	Cathode channel inlet
$\frac{\partial u}{\partial x} = \frac{\partial v}{\partial x} = \frac{\partial w}{\partial z} = 0, \quad \frac{\partial T}{\partial x} = 0$	Anode and cathode channel exit
$\frac{\partial u}{\partial y}_{h_1^-} = \varepsilon_{eff,GDL}\frac{\partial u}{\partial y}_{h_1^+}, \frac{\partial v}{\partial y}_{h_1^-} = \varepsilon_{eff,GDL}\frac{\partial v}{\partial y}_{h_1^+}, \frac{\partial w}{\partial y}_{h_1^-} = \varepsilon_{eff,GDL}\frac{\partial w}{\partial y}_{h_1^+}$	Gas channel and GDL interface
$\varepsilon_{eff,GDL}\frac{\partial u}{\partial y}_{h_2^-} = \varepsilon_{eff,CL}\frac{\partial u}{\partial y}_{h_2^+}, \varepsilon_{eff,GDL}\frac{\partial u}{\partial y}_{h_2^-} = \varepsilon_{eff,CL}\frac{\partial u}{\partial y}_{h_2^+}, \varepsilon_{eff,GDL}\frac{\partial u}{\partial y}_{h_2^-} = \varepsilon_{eff,CL}\frac{\partial u}{\partial y}_{h_2^+}$	GDL and catalyst layer interface
$u = v = w = Ci = 0$	Catalyst layer and membrane interface
$u = v = w = Ci = 0, T_{surface} = 353K$	Top wall of channel
$u = w = 0, T_{surface} = T_{wall}$	Bottom wall of channel
$\phi_{sol} = 0\ , \frac{\partial \phi_{mem}}{\partial y} = 0$	Anode bipolar
$\phi_{sol} = V_{cell}\ , \frac{\partial \phi_{mem}}{\partial y} = 0$	Cathode bipolar
$\frac{\partial \phi_{mem}}{\partial x} = 0, \frac{\partial \phi_{mem}}{\partial z} = 0, \frac{\partial \phi_{sol}}{\partial x} = 0, \frac{\partial \phi_{sol}}{\partial z} = 0$	External surfaces
$u = u_{in}, T = T_{in}, v = 0, C_{H2} = C^{a}_{H2,in}\ ,\ C_{H2O} = C^{a}_{H2O}$	Anode channel inlet
$u = u_{in}, T = T_{in}, v = 0, C_{O2} = C^{c}_{O2,in}\ ,\ C_{N2} = C^{c}_{N2}$	Cathode channel inlet
$\frac{\partial u}{\partial x} = \frac{\partial v}{\partial x} = \frac{\partial w}{\partial z} = 0\ , \quad \frac{\partial T}{\partial x} = 0$	Anode and cathode channel exit
$\frac{\partial u}{\partial y}_{h_1^-} = \varepsilon_{eff,GDL}\frac{\partial u}{\partial y}_{h_1^+}, \frac{\partial v}{\partial y}_{h_1^-} = \varepsilon_{eff,GDL}\frac{\partial v}{\partial y}_{h_1^+}, \frac{\partial w}{\partial y}_{h_1^-} = \varepsilon_{eff,GDL}\frac{\partial w}{\partial y}_{h_1^+}$	Gas channel and GDL interface
$\varepsilon_{eff,GDL}\frac{\partial u}{\partial y}_{h_2^-} = \varepsilon_{eff,CL}\frac{\partial u}{\partial y}_{h_2^+}, \varepsilon_{eff,GDL}\frac{\partial u}{\partial y}_{h_2^-} = \varepsilon_{eff,CL}\frac{\partial u}{\partial y}_{h_2^+}, \varepsilon_{eff,GDL}\frac{\partial u}{\partial y}_{h_2^-} = \varepsilon_{eff,CL}\frac{\partial u}{\partial y}_{h_2^+}$	GDL and catalyst layer interface
$u = v = w = Ci = 0$	Catalyst layer and membrane interface
$u = v = w = Ci = 0, T_{surface} = 353K$	Top wall of channel
$u = w = 0, T_{surface} = T_{wall}$	Bottom wall of channel
$\phi_{sol} = 0\ , \frac{\partial \phi_{mem}}{\partial y} = 0$	Anode bipolar
$\phi_{sol} = V_{cell}\ , \frac{\partial \phi_{mem}}{\partial y} = 0$	Cathode bipolar
$\frac{\partial \phi_{mem}}{\partial x} = 0, \frac{\partial \phi_{mem}}{\partial z} = 0, \frac{\partial \phi_{sol}}{\partial x} = 0, \frac{\partial \phi_{sol}}{\partial z} = 0$	External surfaces

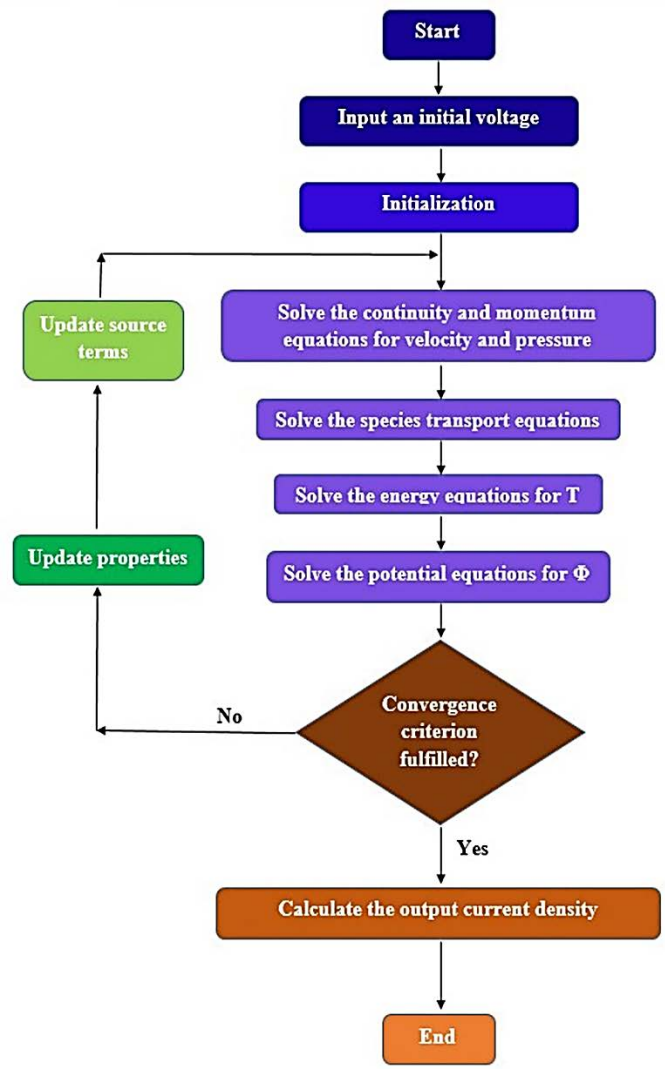

Figure 3. Solution procedure

5. MODEL VALIDATION

To verify the model, numerical results of the base case were compared with the experimental data presented by Ticianelli et al. [13], as shown in Fig. 3a, and there was good agreement between them. Energy unit working conditions and geometric boundaries are given in Table 2. A completely humidified entrance condition is utilized for anode and cathode. The exchange current at anode and cathode can be portrayed by Tafel conditions [11].

Table 2. Geometrical parameters and operating conditions [13]

Parameter	Units	Value
Gas channel length	m	0.05
Gas channel width	m	0.001
Cell width	m	0.002
Gas diffusion layer thickness	m	0.00026
Catalyst layer thickness	m	0.0000129
Membrane thickness	m	0.00023
Cell temperature	K	353.15
Anode pressure	atm	3
Cathode pressure	atm	5

In this model, the organized meshes are utilized and in impetus layers where the electrochemical reactions occur, the lattices are smaller. In addition, a grid freedom test was executed and then, the ideal number of meshes was selected (Figure 4b-c). According to the results, 240000 and 480000 cells have approximately the same output; therefore, for short computation time and fast convergence, 240000 cells were chosen as the best and useful ones.

Figures 5 to 8 show O_2, H_2O, current density, and temperature distributions through the cell width for four cross-sections on the interface between cathode catalyst and membrane layer of 10, 20, 30, and 40 mm in the Z direction for the basic model. Figure 5 shows O_2 mass fractions for two voltages 0.4 and 0.6. It is shown that both trends for graphs are similar, but the value of 0.6 V is slightly more than 0.4 V. A declined process in the mass fraction from z=10 mm to z=40 mm demonstrates an increase in O_2 consumption. This increment causes greater water production for which Figure 6 serves as a clear verification. The current density distribution is presented in Figure 7. It is found that current density is higher at points below the side edges of channels. A temperature graph is observed in Figure 8. It is shown that high temperatures occur in the middle position of the cross line, since, based on Figure 6, the lowest H_2O mass fraction is at that point.

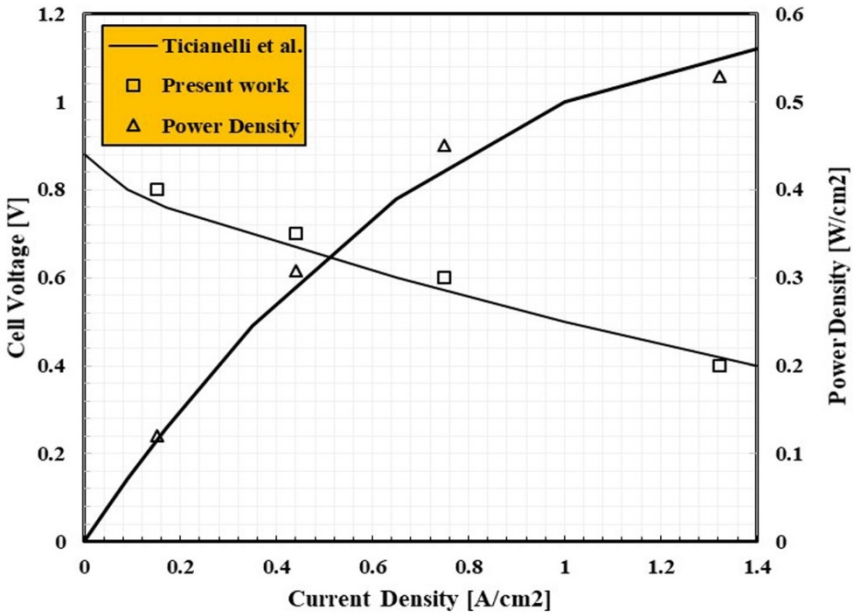

(a)

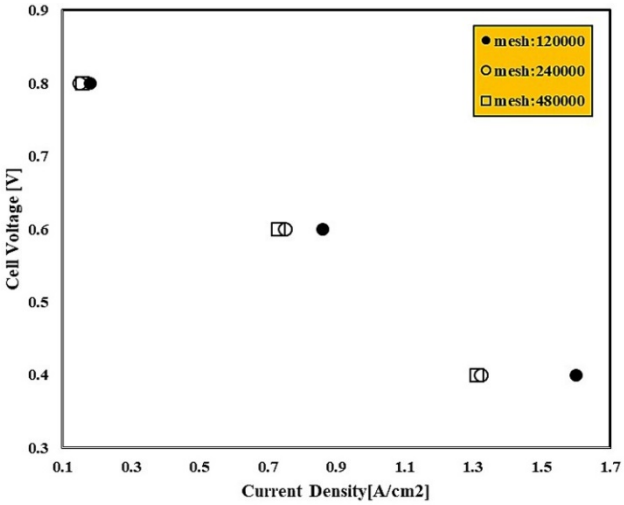

(b)

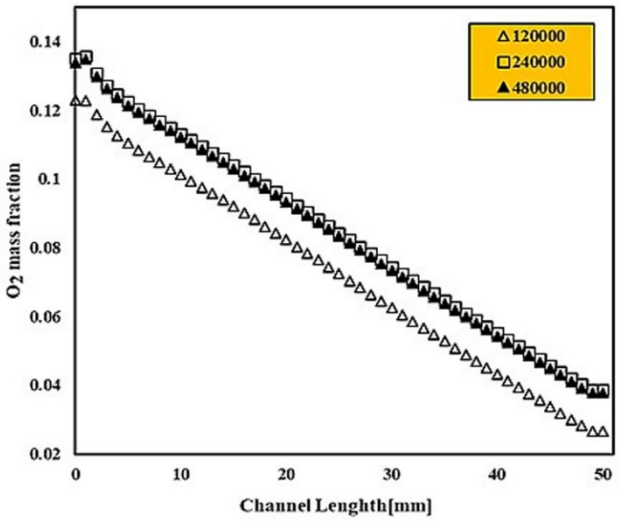

(c)

Figure 4. a) Comparison of experimental data; b) and c) grid independency

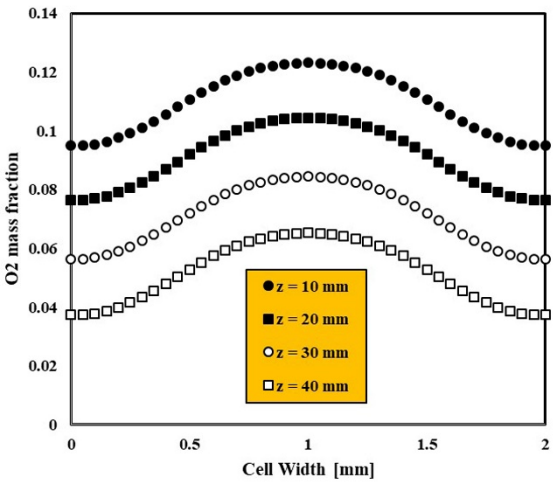

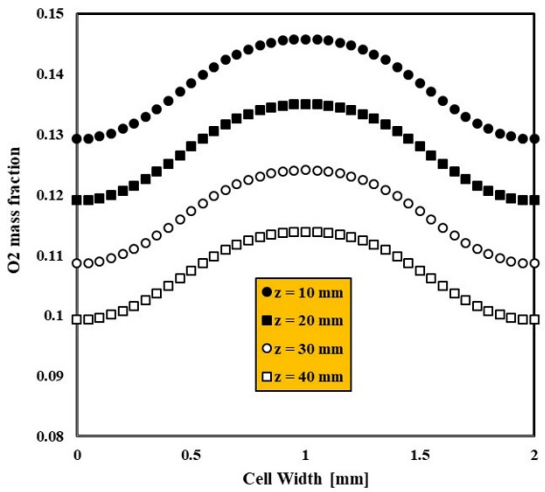

Figure 5. O_2 distribution in the width of the cell for four sections at V=0.4 [V] (Left) and V=0.6 [V] (Right)

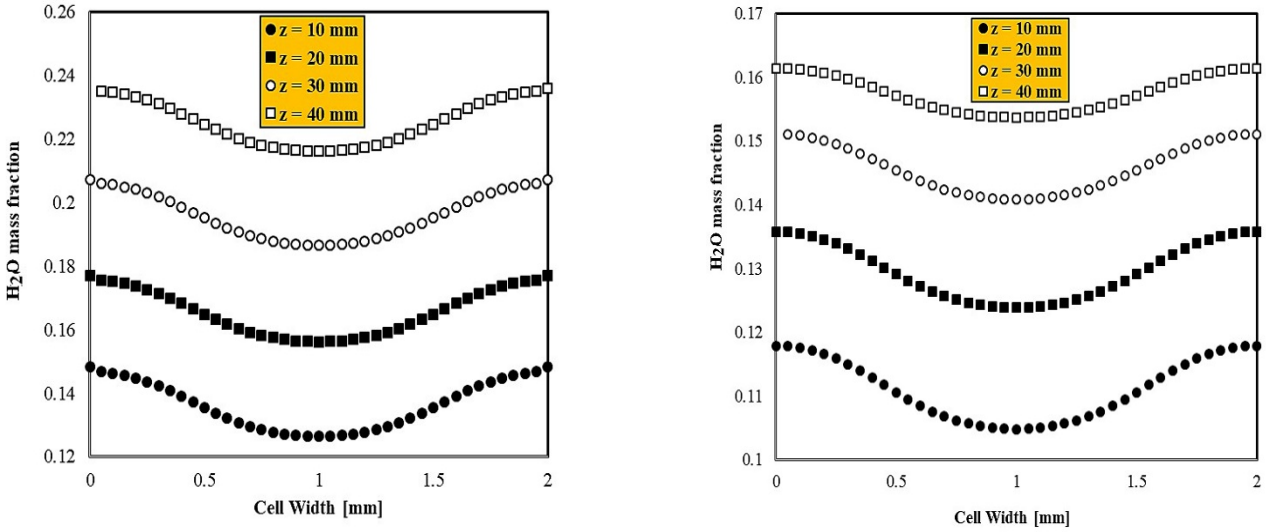

Figure 6. H_2O distribution in the width of the cell for four sections at V=0.4 [V] (Left) and V=0.6 [V] (Right)

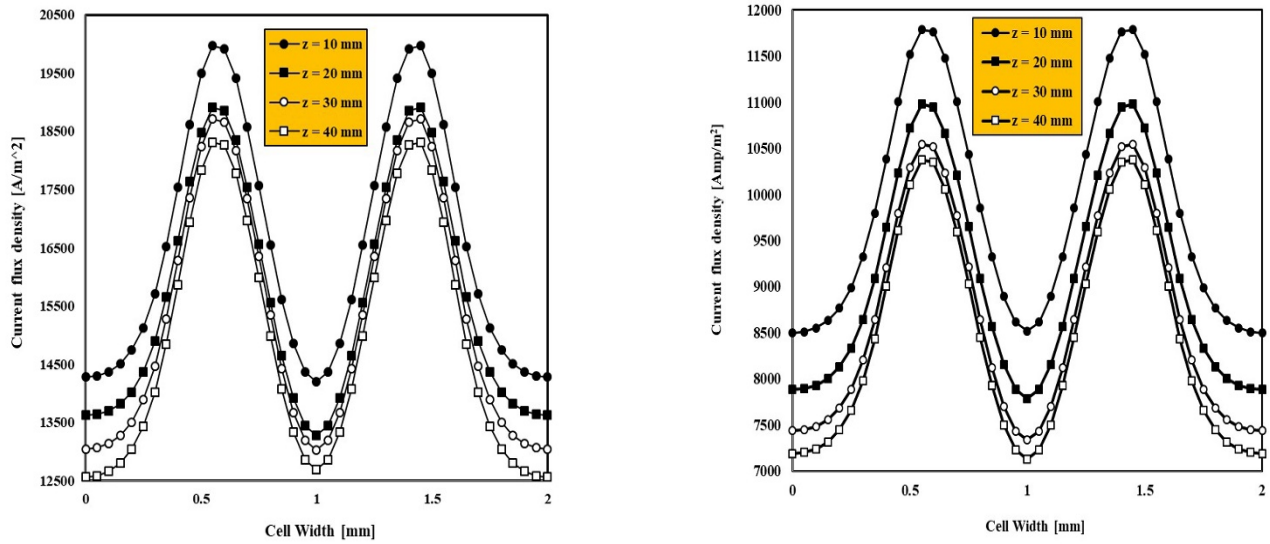

Figure 7. Current density distribution in the width of the cell for four sections at V=0.4 [V] (Left) and V=0.6 [V] (Right)

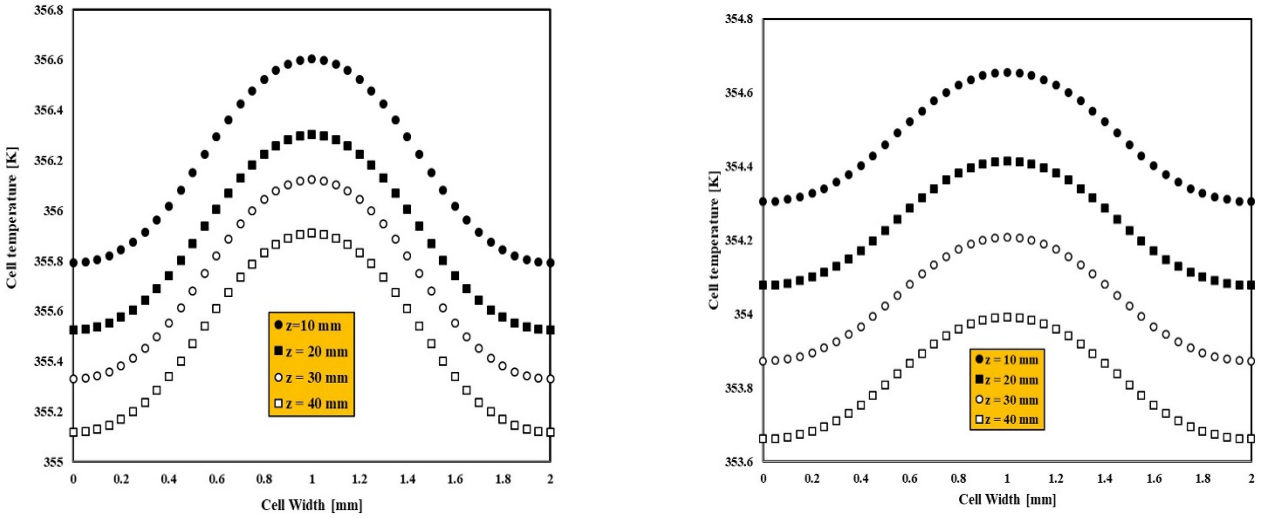

Figure 8. Temperature distribution in the width of the cell for four sections at V=0.4 [V] (Left) and V=0.6 [V] (Right)

5.1. Novel structure of gas channel

In this work, as the new model, a cylindrical fuel cell was simulated. Figure 9b shows a view of this geometry. Figure 10 shows the geometrical characteristic of the novel model. Key parameters such as O_2 and H_2O mass fraction, vathode over potential, temperature, and protonic conductivity were calculated and compared with those in the base model.

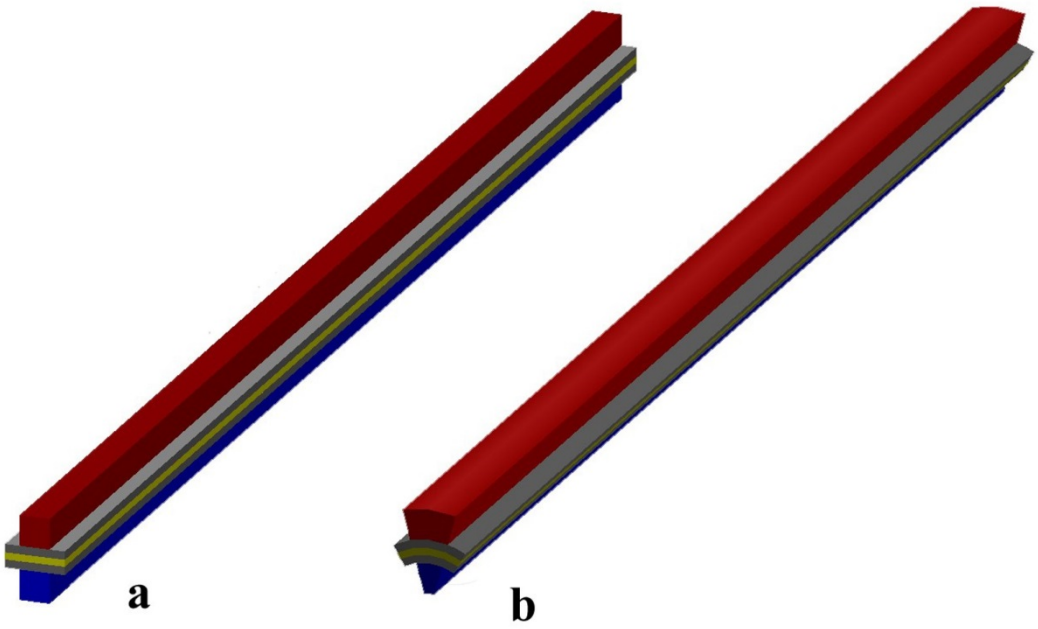

Figure 9. a) base model, b) Cylindrical shape

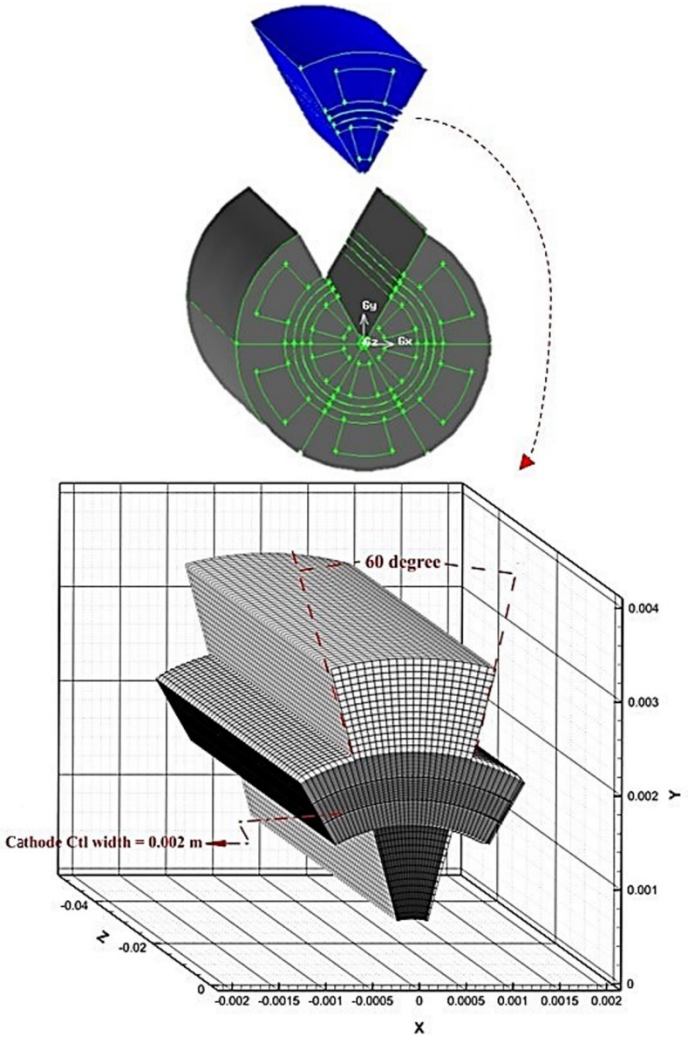

Figure 10. Geometric characteristics of the new model

6. RESULTS AND DISCUSSION

Figures 11 and 12 compare the current density with FC Power for both models, respectively. The cylindrical model operates outperforms the base model. In Table 3, the geometrical conditions of the base and proposed models are presented. Since the cross-section area of the cathode gas channel in the

proposed model is less than that in the base one, according to the continuity equation, the velocity of the incoming gas flow will be higher. In doing so, diffusion of oxygen to the electrochemical reaction area is enhanced. Consequently, the new model outperforms the base model. Figures 13 to 16 show the distribution graph and contour of H_2O mass fraction for both models. Water production in the novel model is greater than that in the base model. Figures 17 to 20 are about O_2 mass fraction. It is observed that O_2 consumption increases through the channel from the entrance to the exit point in the base model and it increases to a greater degree in the middle points of the channel.

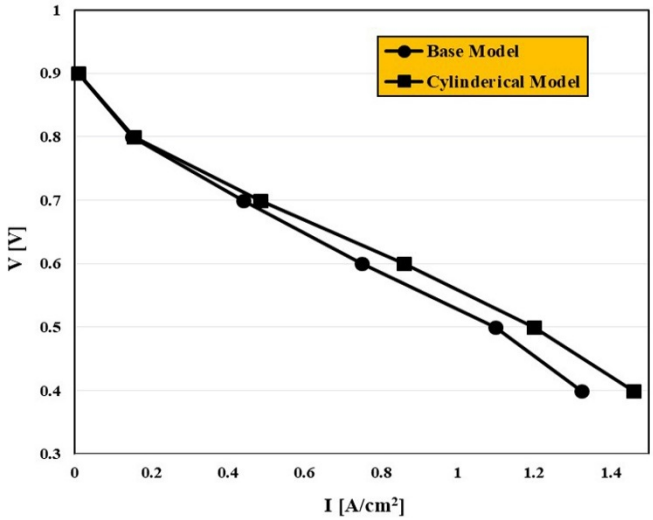

Figure 11. Current density for both models

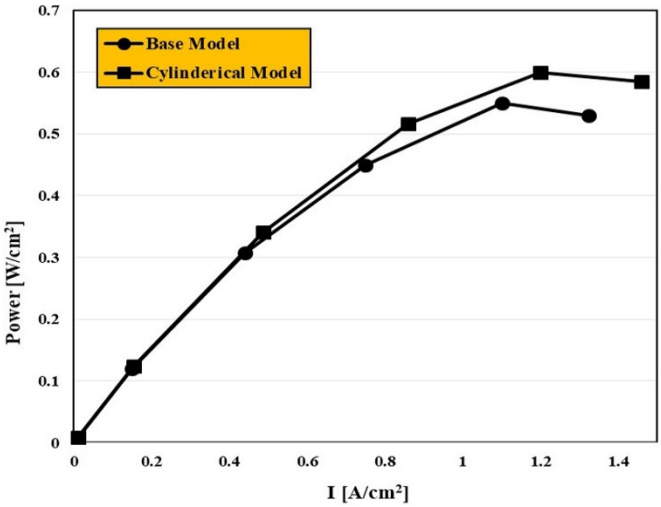

Figure 12. Fuel cell power for both models

Table 3. Geometrical condition of the novel model

	Units	Base model	Proposed model
Cathode gas channel area	m^2	10^{-6}	5.95×10^{-7}
Anode gas channel area	m^2	10^{-6}	2.12×10^{-6}
Reaction area	m^2	10^{-4}	10^{-4}

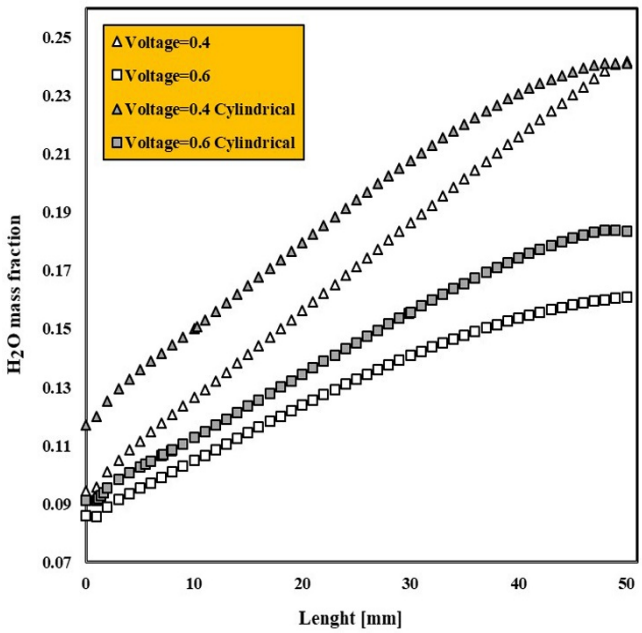

Figure 13. H_2O mass fraction through cathode catalyst layer for both models

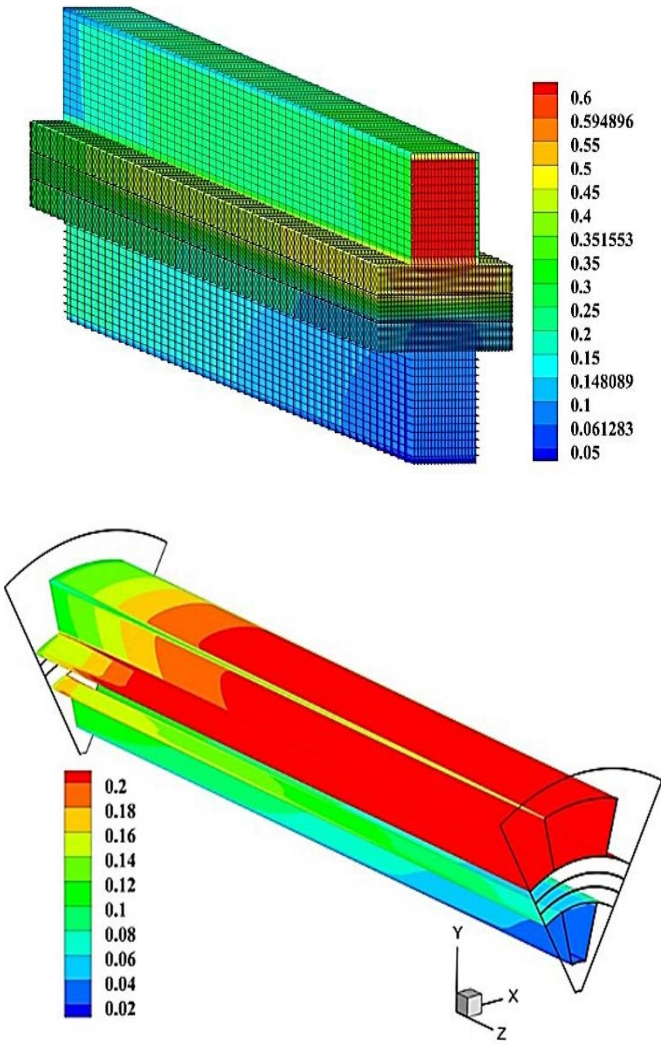

Figure 14. 3D H_2O contour for V=0.4 [V]: The base model (top) and the proposed model (bottom)

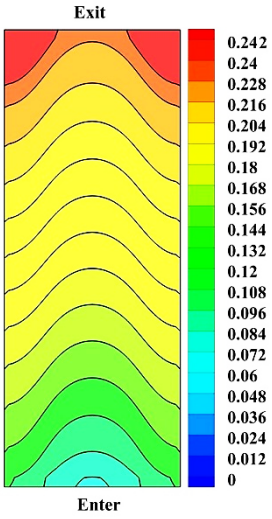

Base model. V = 0.4 [V]

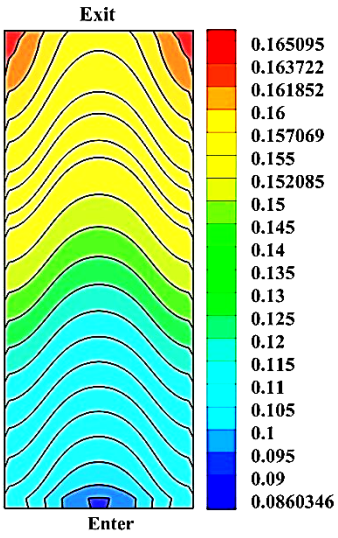

Base model. V= 0.6 [V]

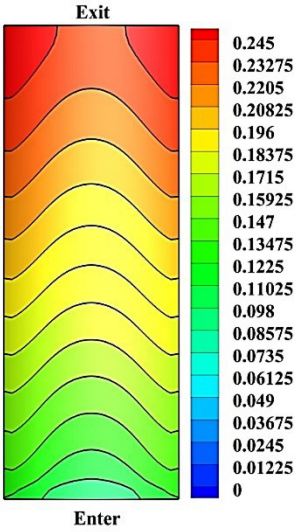

Cylindrical model. V = 0.4 [V]

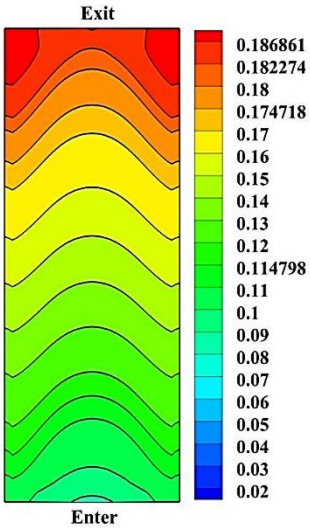

Cylindrical model. V= 0.6 [V]

Figure 15. H_2O mass fraction contours through the cathode catalyst layer for both models

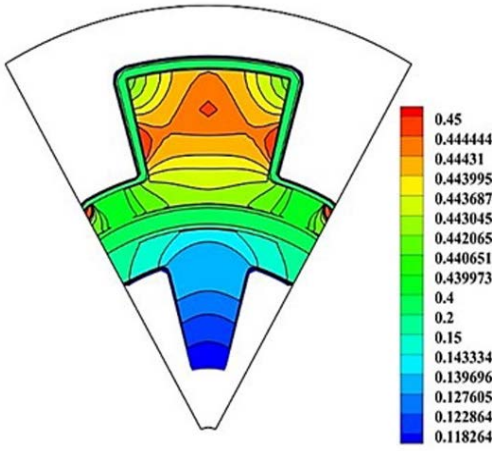

Cylindrical model. V= 0.4 [V]

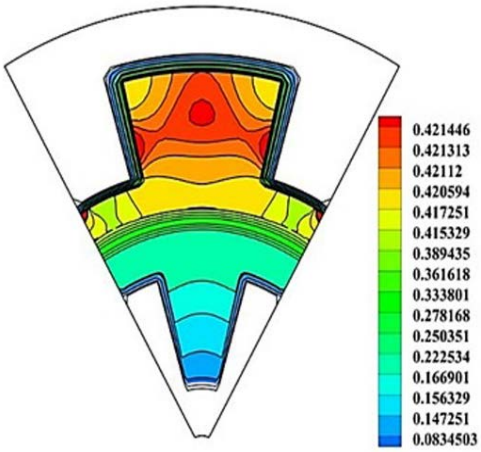

Cylindrical model. V= 0.6 [V]

Figure 16. H_2O mass fraction contours for the cylindrical models at z = 25 mm

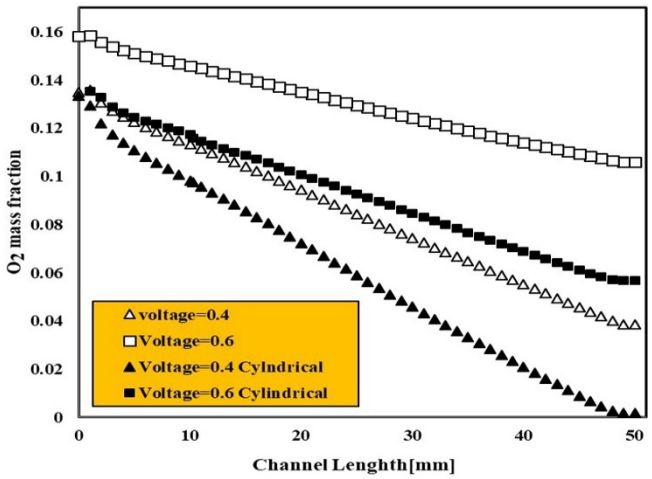

Figure 17. O_2 mass fraction through the cathode catalyst layer for both models

Figure 20 shows the contour of O_2 mass fraction for both voltages in a cross-section at z = 25 mm. It is observed that O_2 consumption mostly occurs near the membrane layer. In the same procedure, Figure 16 shows the H_2O mass fraction through the cell width.

Figure 21 is a temperature contour for four cross-sections in the cylindrical model in the case of both voltages. Additionally, a contour is shown at z = 25 mm. As mentioned before, the lower the water mass fraction, the higher the temperature, which is in the middle of the cell as shown in the contours. In addition, Figure 22 is a line graph for temperature through the cell length. According to this figure, the temperature at low voltage is greater than that at high voltage and its value is higher in the new cylindrical model.

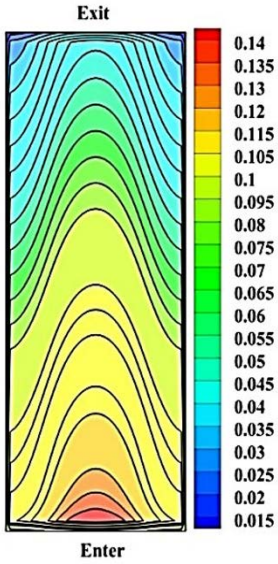

Base model. V= 0.4 [V]

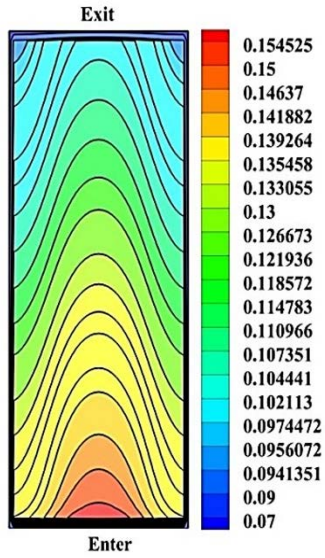

Base model. V= 0.6 [V]

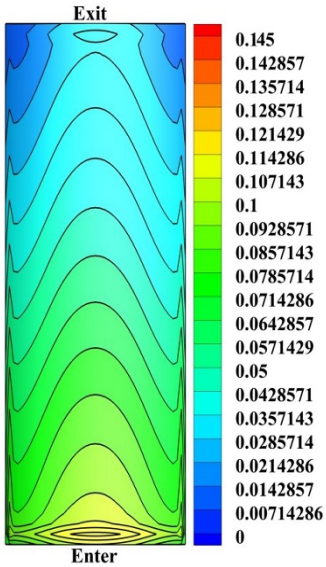

Cylindrical model. V= 0.4 [V]

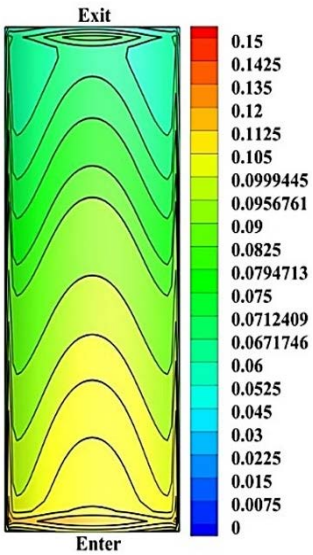

Cylindrical model. V= 0.6 [V]

Figure 18. O_2 mass fraction contours through the cathode catalyst layer for both models

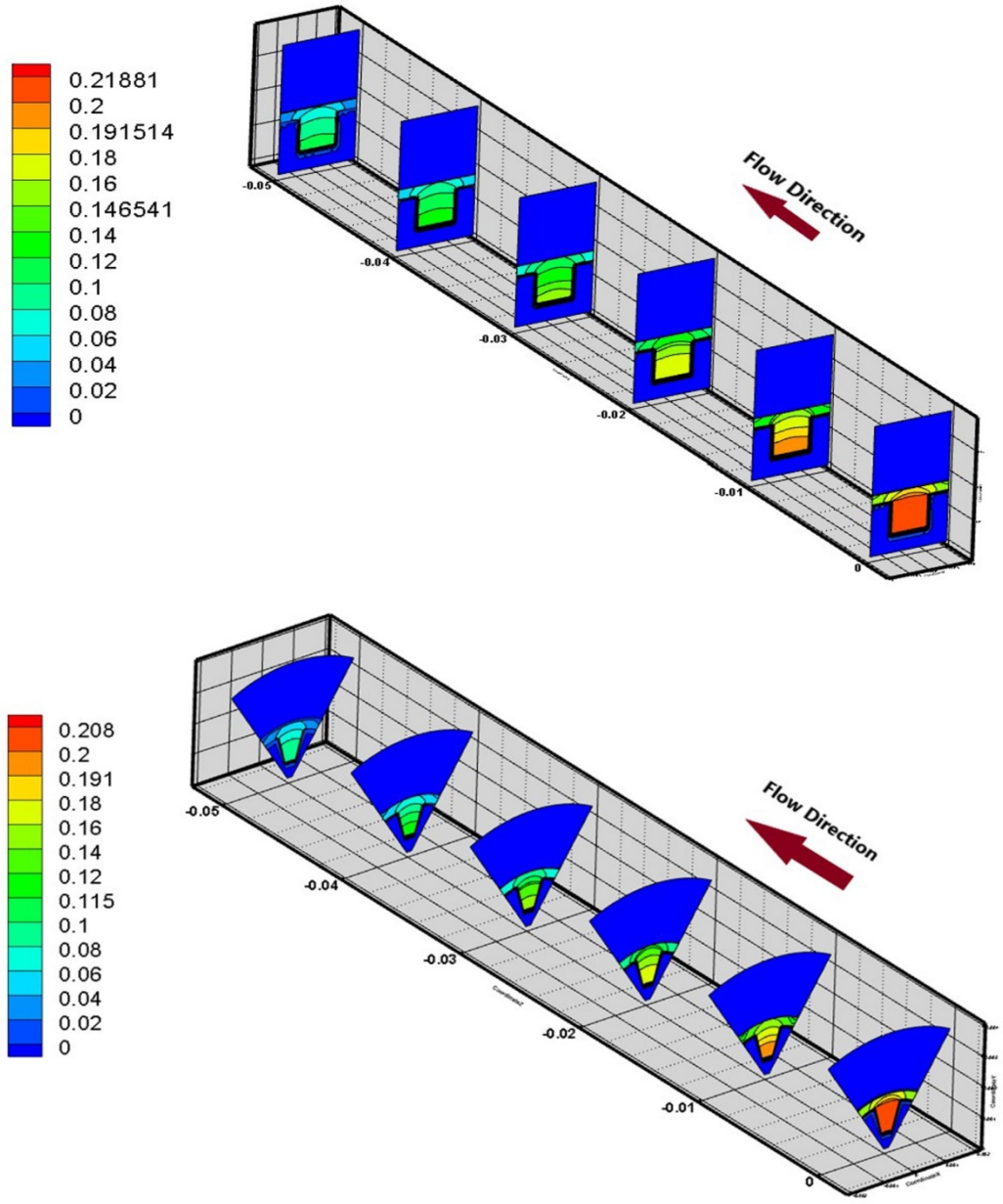

Figure 19. 3D O_2 contour for both model for V=0.4 [V]

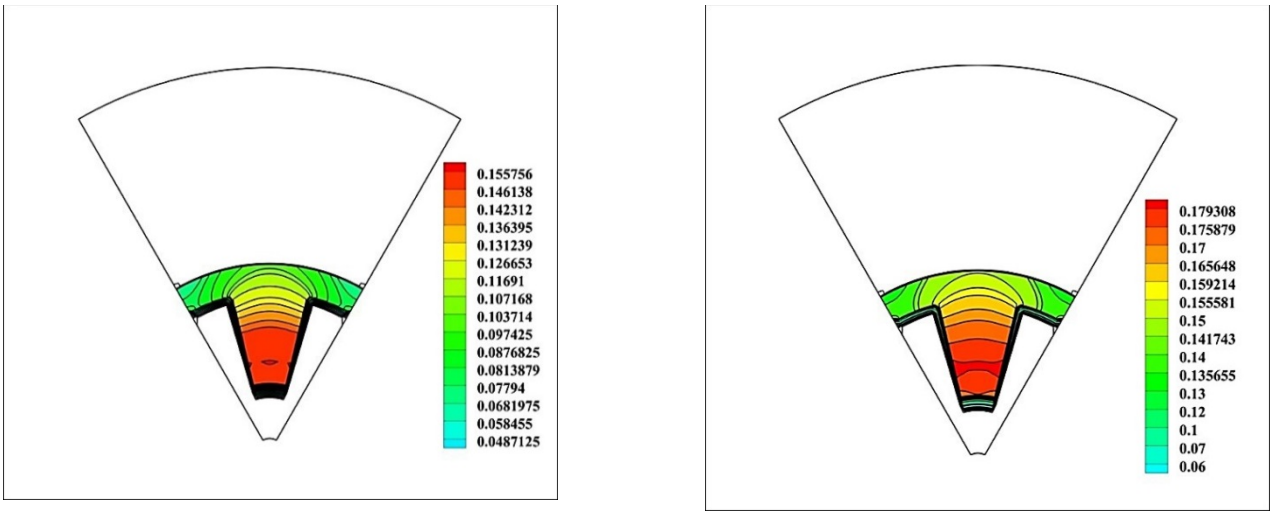

Cylindrical model. V= 0.4 [V] Cylindrical model. V= 0.6 [V]

Figure 20. O_2 mass fraction contours for cylindrical models at z = 25 mm

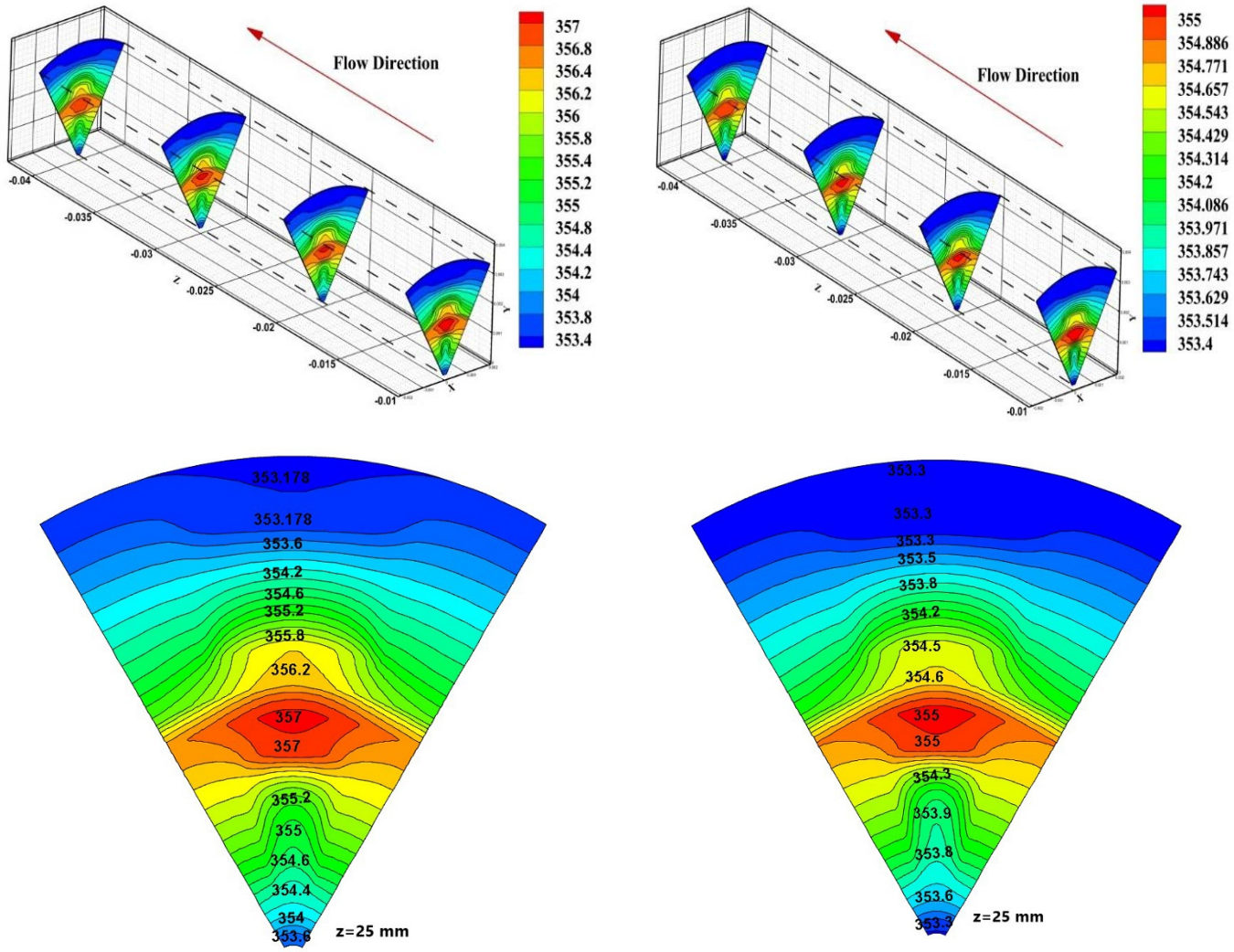

Figure 21. Temperature contours for cylindrical models at V= 0.4 [V] (Left) and V= 0.6 [V] (Right)

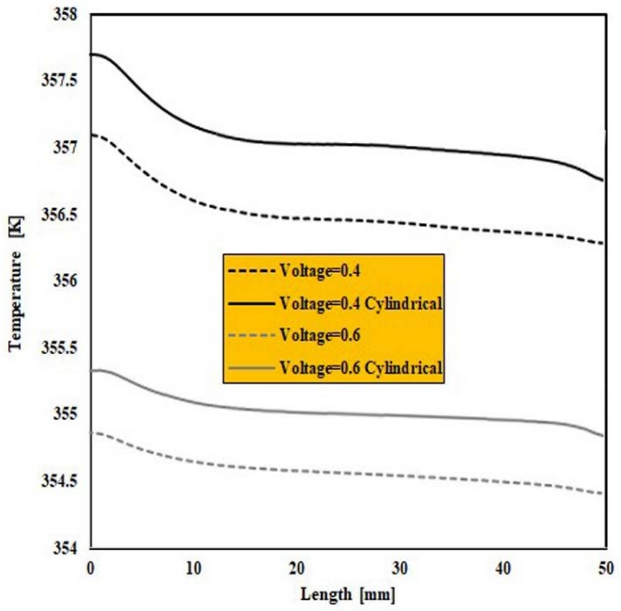

Figure 22. Cell temperature through the cathode catalyst layer for both models

Figure 23 shows H_2 mass fractions for the anode zone. This figure certifies previous tips.

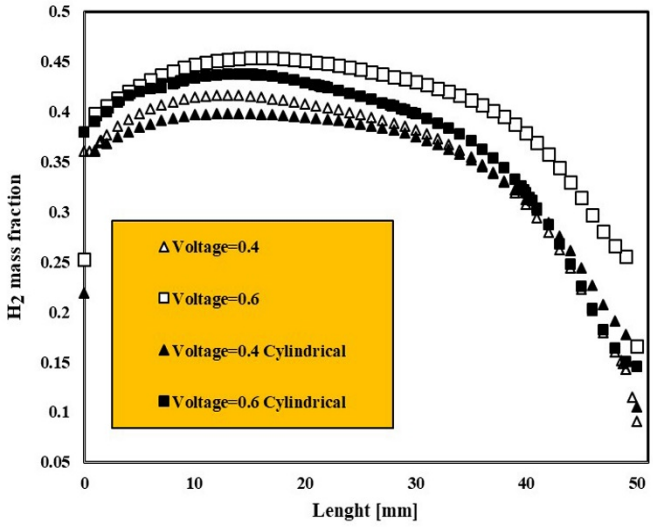

Figure 23. Anode H_2 mass fraction for both models

Cathode Protonic Conductivity (CPC) is an important parameter of water distribution, as shown in Figure 24. Cathode Over Potential (COP) parameter considerably corresponds to the amount of O_2. The less oxygen there is, the greater COP factor will be, as shown in Figure 25.

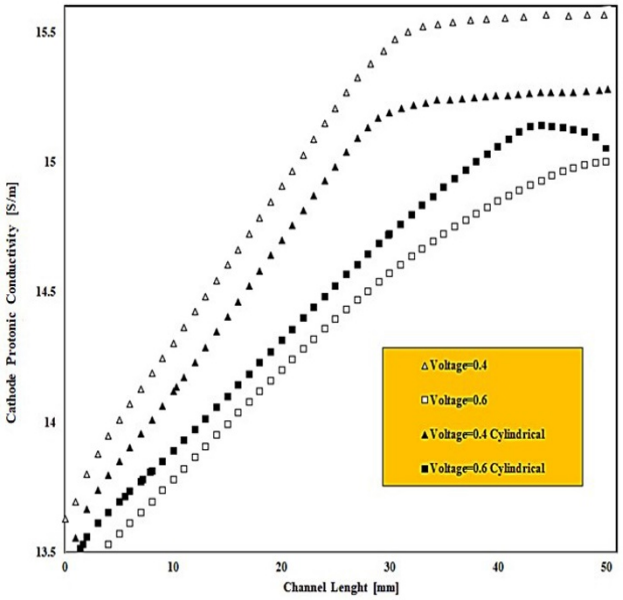

Figure 24. CPC parameter for both models

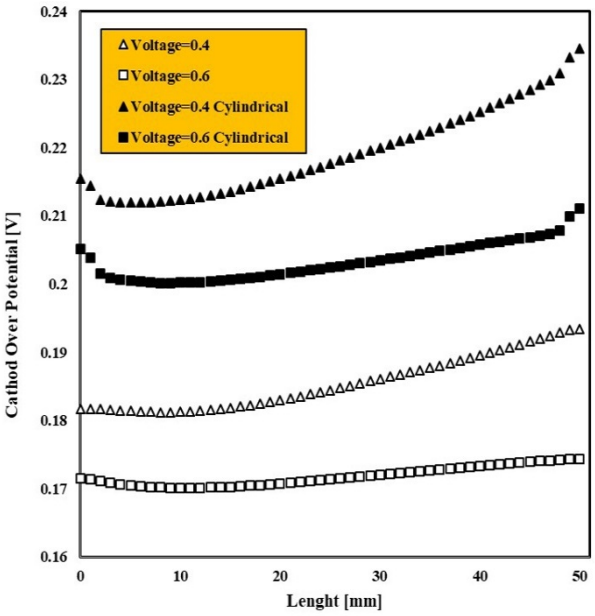

Figure 25. COP parameter for both models

As shown in Figure 25, it is found that the COP factor at low voltage is quite significant and the cylindrical configuration has a higher value for COP. Figures 26 and 27 show the current density distribution graph through the cell length and contours related to this parameter for both models. It is found that the novel model is endowed with higher efficiency, meaning that this model has greater current density and significant performance.

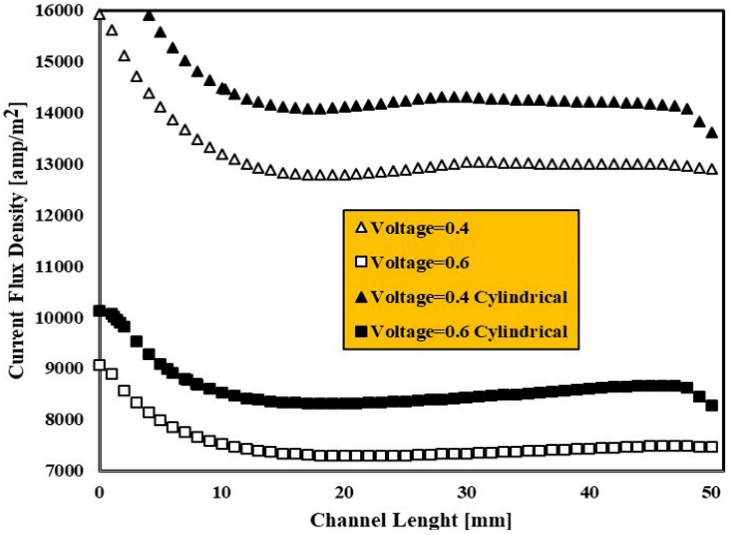

Figure 26. Current density for both models

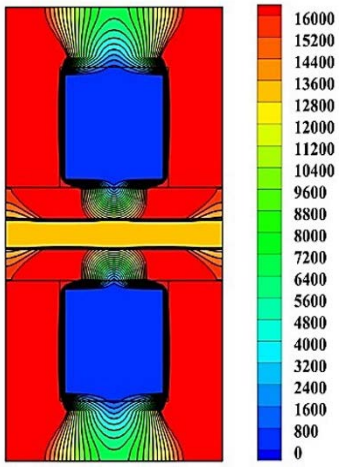

Base model. V= 0.4 [V]

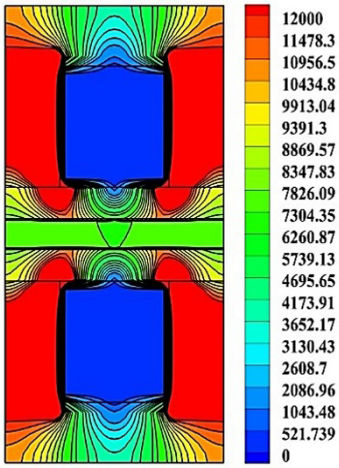

Base model. V= 0.6 [V]

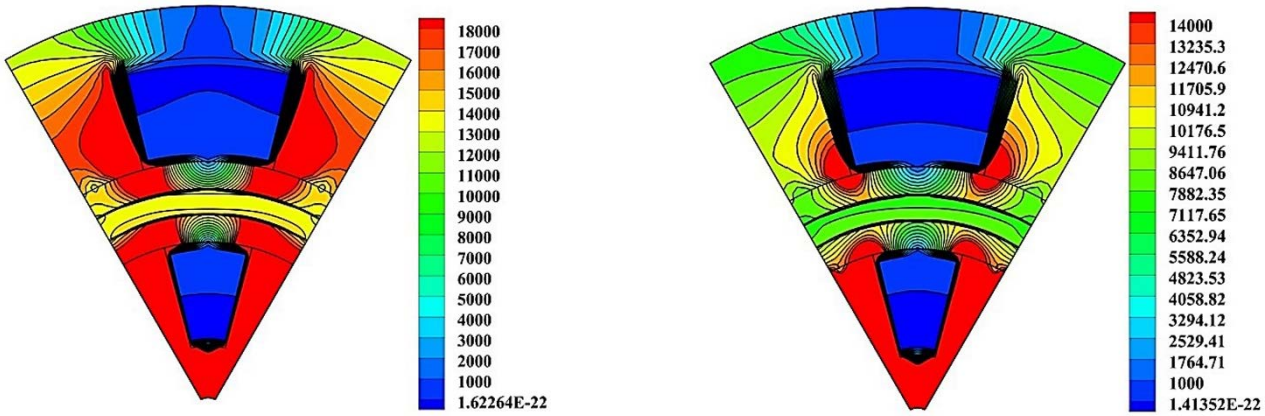

Cylindrical model. V= 0.4 [V] Cylindrical model. V= 0.6 [V]

Figure 27. Current density contours for both models

7. CONCLUSIONS

In the present work, a base model and the novel geometry of PEM fuel cells were numerically simulated. Finite Volume Method (FVM) was used for discretizing the governing equations. Validation of obtained numerical results was done and good agreement was concluded. The results showed that the new proposed model extracted higher electrical current density (10.35 %) than the base model at V=0.4 [V], and the average increment in generated power was about 8 %, which could be a considerable value in a stack of cells. Moreover, the oxygen and hydrogen consumption and consequently, water production and heat generation were quite high under the new model. In addition, it can be mentioned that the COP factor at low voltage was significantly high and the cylindrical configuration had a higher value for COP.

8. FUTURE RECOMMENDATION

As a future recommendation, some points can be represented as follows:

- Changing the cathode and anode zones and studying the corresponding effect on cell performance.
- Considering the same channel cross-section for both configurations instead of the same reaction area and comparing the results with each other.
- Utilizing ethane, methane, and propane as fuels for cell and investigating the effect of C presence in reactions.

9. ACKNOWLEDGEMENT

We gratefully acknowledge the Urmia University of Technology computer center manager for allowing us to use their computers.

REFERENCES

1. Fuel cells, Editor: Kreuer, K.-D., Springer, New York, (2013). (https://doi.org/10.1007/978-1-4614-5785-5).
2. Bernardi, D.M. and Verbrugge, M.W., "Mathematical model of a gas discussion electrode bonded to a polymer electrolyte", ***American Institute of Chemical Engineers Journal***, Vol. 37, No. 8, (1991), 1151-1163. (https://doi.org/10.1002/aic.690370805).
3. Bernardi, D.M. and Verbrugge, M.W., "A mathematical model of the solid-polymer-electrolyte fuel cell", ***Journal of Electrochemical Society***, Vol. 139, No. 9, (1992), 2477-2491. (https://doi.org/10.1149/1.2221251).
4. Fuller, T.F. and Newman, J., "Water and thermal management in solid-polymer-electrolyte fuel cells", ***Journal of Electrochemical Society***, Vol. 140, No. 5, (1993), 1218-1225. (https://doi.org/10.1149/1.2220960).
5. Nguyen, T.V. and White, R.E., "Water and heat management model for proton-exchange-membrane fuel cells", ***Journal of the Electrochemical Society***, Vol. 140, (1993), 2178-2186. (https://doi.org/10.1149/1.2220792).
6. Dutta, S., Shimpalee, S. and Van Zee, J.W., "Three-dimensional numerical simulation of straight channel PEM fuel cells", ***Journal of Applied Electrochemistry***, Vol. 30, (2000), 135-146. (https://doi.org/10.1023/a:1003964201327).
7. Berning, T. and Djilali, N., "Three-dimensional computational analysis of transport phenomena in a PEM fuel cell: A parametric study", ***Journal of Power Source***, Vol. 124, (2003), 440-452. (https://doi.org/10.1016/s0378-7753(03)00816-4).
8. Yang, T., Park, G., Pugazhendhi, P., Lee, W. and Kim, C.S., "Performance improvement of electrode for polymer electrolyte membrane fuel cell", ***Korean Journal of Chemical Engineering***, Vol. 19, No. 3, (2002), 417-420. (https://doi.org/10.1007/bf02697149).
9. Molaeimanesh, G.R. and Akbari, M.H., "Water droplet dynamic behavior during removal from a proton exchange membrane fuel cell gas diffusion layer by Lattice-Boltzmann method", ***Korean Journal of Chemical Engineering***, Vol. 31, No. 4, (2014), 598-610. (https://doi.org/10.1007/s11814-013-0282-6).
10. Carral, C. and Mélé, P., "A numerical analysis of PEMFC stack assembly through a 3DFinite element model", ***International Journal of Hydrogen Energy***, Vol. 39, No. 9, (2014), 4516-4530. (https://doi.org/10.1016/j.ijhydene.2014.01.036).
11. Ahmadi, N., Dadvand, A., Rezazadeh, S. and Mirzaee, I., "Analysis of the operating pressure and GDL geometrical configuration effect on PEM fuel cell performance", ***Journal of the Brazilian Society of Mechanical Sciences and Engineering***, Vol. 38, (2016), 2311-2325. (https://doi.org/10.1007/s40430-016-0548-0).
12. Rezazadeh, S. and Ahmadi, N., "Numerical investigation of gas channel shape effect on proton exchange membrane fuel cell performance", ***Journal of the Brazilian Society of Mechanical Sciences and Engineering***, Vol. 37, (2017), 789-802. (https://doi.org/10.1007/s40430-014-0209-0).
13. Ticianelli, E.A., Derouin, C.R., Redondo, A. and Srinivasan, S., "Methods to advance technology of proton exchange membrane fuel cell", ***Journal of The Electrochemical Society***, Vol. 135, No. 9, (1988), 2209-2214. (https://doi.org/10.1149/1.2096240).
14. Ahmadi, N., Pourmahmoud, N., Mirzaee, I. and Rezazadeh, S., "Three-dimensional computational fluid dynamic study of the effect of the different channel and shoulder geometries on cell performance", ***Australian Journal of Basic and Applied Sciences***, Vol. 5, No. 12, (2011), 541-556. (http://www.ajbasweb.com/old/ajbas/2011/December-2011/541-556.pdf).
15. Ahmadi, N., Rezazadeh, S., Mirzaee, I., and Pourmahmoud, N., "Three-dimensional computational fluid dynamic analysis of the conventional PEM fuel cell and investigation of prominent gas diffusion layers effect", ***Journal of Mechanical Science and Technology***, Vol. 26, No. 8, (2012), 2247-2257. (https://doi.org/10.1007/s12206-012-0606-1).
16. Lin, W., Husar, A., Zhou, T. and Liu, H., "A parametric study of PEM fuel cell performances", ***International Journal of Hydrogen Energy***,

Vol. 28, No. 11, (2003), 1263-1272. (https://doi.org/10.1016/s0360-3199(02)00284-7).

17. Ahmadi, N., Rezazadeh, S. and Mirzaee, I., "Study the effect of various operating parameters of proton exchange membrane", ***Periodica Polytechnica. Chemical Engineering***, Vol. 59, No. 3, (2015), 221-235. (https://doi.org/10.3311/ppch.7577).
18. Ahmadi, N., Rezazadeh, S., Dadvand, A. and Mirzaee, I., "Numerical investigation of the effect of gas diffusion layer with semicircular prominences on polymer exchange membrane fuel cell performance and species distribution", ***Journal of Renewable Energy and Environment (JREE)***, Vol. 2, No. 2, (2015), 36-46. (https://doi.org/10.30501/JREE.2015.70069).
19. Ahmadi, N., Rezazadeh, S., Dadvand, A. and Mirzaee, I., "Modelling of gas transport in proton exchange membrane fuel cells", ***Institution of Civil Engineers***, Vol. 170, No. 4, (2017), 163-179. (https://doi.org/10.1680/jener.15.00015).
20. Ahmadi, N., Dadvand, A., Rezazadeh, S. and Mirzaee, I., "Modeling of polymer electrolyte membrane fuel cell with circular and elliptical cross-section gas channels: A novel procedure", ***International Journal of Energy Research***, Wiley, (2018). (https://doi.org/10.1002/er.4069).
21. Pashaee Golmarz, T., Rezazadeh, S. and Bagherzadeh, N., "Numerical study of curved-shape channel effect on performance and distribution of species in a proton-exchange membrane fuel cell: Novel structure", ***Journal of Renewable Energy and Environment (JREE)***, Vol. 5, No. 2, (2018), 10-21. (https://doi.org/10.30501/JREE.2018.88506).
22. Zunyan, H., Liangfei, X., Jianqiu, L., Qing, W., Yangbin, Sh., Xiaojing, Ch., Wei, D. and Minggao, O., "Mechanistic insight into the accelerated decay of fuel cells from catalyst-layer structural failure", ***Energy Conversion, and Management***, Vol. 227, (2021), 113568. (https://doi.org/10.1016/j.enconman.2020.113568).
23. Olabi, A., Wilberforce, T. and Abdelkareem, M., "Fuel cell application in the automotive industry and future perspective", ***Energy***, Vol. 214, (2021), 118955. (https://doi.org/10.1016/j.energy.2020.118955).
24. Xun, Zh., Yuan, Zh., Ding-Ding, Y., Rong, Ch., Tong, Zh. and Qiang, L., "Discrete-holes film fueling anode heads for high performance air-breathing microfluidic fuel cell", ***Journal of Power Sources***, Vol. 482, (2021), 228966. (https://doi.org/10.1016/j.jpowsour.2020.228966).
25. Chen, K., Laghrouche, S. and Djerdir, A., "Performance analysis of PEM fuel cell in the mobile application under real traffic and environmental conditions", ***Energy Conversion and Management***, Vol. 227, (2021), 113602. (https://doi.org/10.1016/j.enconman.2020.113602).